

Structure and dynamics of the Martian lower and middle atmosphere as observed by the Mars Climate Sounder:

2. Implications of the thermal structure and aerosol distributions for the mean meridional circulation

N. G. Heavens,^{1,2} D. J. McCleese,³ M. I. Richardson,⁴ D. M. Kass,³ A. Kleinböhl,³ and J. T. Schofield³

Received 13 August 2010; revised 11 November 2010; accepted 29 November 2010; published 28 January 2011.

[1] Retrievals of temperature, dust, and water ice from data collected by the Mars Climate Sounder (MCS) on Mars Reconnaissance Orbiter (MRO) illustrate for the first time the seasonal and diurnal variability of both the thermal structure of the middle atmosphere (above 40 km) and also the vertical distribution of aerosols. These retrievals reveal clear signatures of significant mean meridional cells in the middle and lower atmosphere at both the solstices and equinoxes. We investigate the degree to which the lower and middle atmospheric circulations are kinematically coupled and conclude that kinematic coupling is strong in the tropics throughout the year but weak near the pole except during the “polar warming” events associated with dust storm activity.

Citation: Heavens, N. G., D. J. McCleese, M. I. Richardson, D. M. Kass, A. Kleinböhl, and J. T. Schofield (2011), Structure and dynamics of the Martian lower and middle atmosphere as observed by the Mars Climate Sounder: 2. Implications of the thermal structure and aerosol distributions for the mean meridional circulation, *J. Geophys. Res.*, *116*, E01010, doi:10.1029/2010JE003713.

1. Introduction

[2] The atmosphere of Mars is conventionally divided into three broad layers with quantitatively indistinct but qualitatively defined boundaries: the lower atmosphere, the middle atmosphere, and the upper atmosphere. In the classification scheme expounded by Zurek [1992], lapse rates are strongly positive (1–4.5 K km⁻¹) in the lower atmosphere due to the vertical transport of heat from the surface by radiation, conduction, and advection; are weakly positive or isothermal in the middle atmosphere due to infrared cooling of CO₂; and become negative (<-1 K km⁻¹) at the base of the upper atmosphere (~100 km above the surface) due to molecular conduction of heat downward from the layer strongly absorbing solar extreme ultraviolet (EUV) radiation. (“Lapse rate” refers here to the rate of decrease of atmospheric temperature with height.) Zurek [1992] argues that the boundary between the lower and the middle atmosphere is necessarily indistinct, because the extent of strongly positive lapse rates is dependent on the vertical distribution of dust, which varies widely both seasonally and interannually, but places the

average height of the boundary at ~45 km above the surface and at an atmospheric pressure of ~10 Pa. In addition, the momentum budgets of these two layers may differ considerably. The lower atmosphere’s momentum budget may be strongly dominated by interactions with the surface and baroclinic waves just like the Earth’s troposphere, while the middle atmosphere’s momentum budget may be dominated by the dissipation of gravity waves and tides just like the Earth’s mesosphere [e.g., Barnes, 1991].

[3] The thermal structure of the lower atmosphere has been measured systematically over several Martian years by a combination of infrared nadir sounding by instruments such as the Viking Infrared Thermal Mapper (IRTM) [Clancy *et al.*, 2000] and the Thermal Emission Spectrometer (TES) on Mars Global Surveyor (MGS) [Smith *et al.*, 2001] and radio occultation measurements by the Radio Science Experiment on MGS [Hinson *et al.*, 1999]. The thermal structure of the upper atmosphere has been measured using accelerometer data from orbiting spacecraft [e.g., Bougher *et al.*, 1999] and observations of ultraviolet light from stars occulted by the atmosphere [Forget *et al.*, 2009]. Yet until recently, information about the thermal structure and circulation of the middle atmosphere were limited to ground-based microwave observations [e.g., Deming *et al.*, 1986] and a limited number of retrievals from infrared limb observations by TES.

[4] New observations by the Mars Climate Sounder (MCS) [McCleese *et al.*, 2007] on Mars Reconnaissance Orbiter (MRO) [Zurek and Smrekar, 2007] are now providing information about the thermal structure of Mars over both the

¹Division of the Geological and Planetary Sciences, California Institute of Technology, Pasadena, California, USA.

²Now at the Department of Earth and Atmospheric Sciences, Cornell University, Ithaca, New York, USA.

³Jet Propulsion Laboratory, California Institute of Technology, Pasadena, California, USA.

⁴Ashima Research, Pasadena, California, USA.

lower atmosphere and middle atmosphere, and at higher spatial and temporal resolution than previously available. In addition, observations from MCS have been used to retrieve vertical profiles of aerosol, which help to constrain the lower atmospheric circulation and the forcing of the circulation by radiative heating/cooling due to dust and water ice.

[5] Among other uses, MCS retrievals can validate numerical models of the Martian atmosphere and identify atmospheric processes that may explain discrepancies encountered in validation. While numerical models of the Earth's atmosphere for climate studies and weather prediction typically have vertical domains that stop in the middle of the stratosphere, numerical models used for climate studies and planning for the descent of spacecraft to the Martian surface require vertical domains similar to that of MCS.

[6] It has been observed that during some regional Martian dust storms, atmospheric temperatures at approximately 15 to 35 km above the winter northern pole dramatically warm over the course of a few Martian days by up to 80 K [*Jakosky and Martin*, 1987]. While warming at midlatitudes can be explained by direct solar heating of dust advected from the southern hemisphere or the northern tropics, the warming within the polar night cannot be due to the absorption of solar radiation. Instead, it has been attributed to adiabatic heating from strong downwelling over the pole, in particular downwelling of the principal meridional overturning cell (PMOC) [*Haberle et al.*, 1982; *Schneider*, 1983; *Haberle et al.*, 1993].

[7] When the first wave-resolving, three-dimensional model of the Martian general circulation was developed in the early 1990s [*Haberle et al.*, 1993], it could not simulate dust storm polar warmings, since the downwelling of the simulated PMOC never penetrated further than 65° to 70°N, which *Haberle et al.* [1993] attributed to insufficiently strong eddy transport of heat and momentum. *Wilson* [1997] successfully simulated a dust storm polar warming with a Mars general circulation model (GCM) by using a deeper vertical domain than used by *Haberle et al.* [1993] and by resolving the atmospheric thermal tides. The deep vertical domain reduced the sensitivity of the simulation to dissipation at the model top and vertically resolved the PMOC and the atmospheric thermal tides during the dust storm. The atmospheric thermal tides transported sufficient angular momentum to drive the PMOC downwelling closer to the north pole. The resulting circulation strongly upwelled at the surface near the south pole, vigorously crossed the equator at altitudes as high as 70 km above the surface, strongly downwelled near the north pole, and returned toward the south pole near the surface, forming a “pole-to-pole” PMOC first proposed by *Schneider* [1983]. Other GCM simulations by *Forget et al.* [1999] and *Kuroda et al.* [2009] differ from that of *Wilson* [1997] with respect to the atmospheric dust levels or wave forcings necessary to produce a polar warming event, but both simulations produce latitudinally broad and vertically deep mean meridional circulations. Thus, in order to ensure that such a cell can be vertically resolved, current Martian GCMs [e.g., *Wilson and Hamilton*, 1996; *Forget et al.*, 1999; *Takahashi et al.*, 2003; *Moudden and McConnell*, 2005; *Angelats i Coll et al.*, 2005; *Hartogh et al.*, 2005; *Kuroda et al.*, 2005; *Kahre et al.*, 2006; *Richardson et al.*, 2007] generally simulate both the lower and middle atmosphere.

[8] Dust storm polar warmings are exceptional events, so it is not likely that the PMOC regularly extends to 70 km

above the surface. However, observations by TES and MCS [*McCleese et al.*, 2008] and modeling by *Forget et al.* [1999], *Kuroda et al.* [2005], and *Hartogh et al.* [2007] (among others) suggest that there may be weaker polar thermal inversions in the middle atmosphere outside of dust storm conditions.

[9] The underlying dynamics of these inversions are murky. *McCleese et al.* [2008] claim that an inversion in the middle atmosphere near the south pole during its winter is “consistent with the behavior of a Hadley circulation in which the polar warming is the result of compressional heating in the descending branch of the mean meridional overturning circulation” and thus imply that the PMOC penetrates to high altitudes above the southern winter pole, much like in a dust storm polar warming. Yet the weakness of the southern winter polar inversion relative to the dust storm polar warmings is never explained.

[10] *McCleese et al.* [2008] also propose that models generally underestimate the magnitude of southern winter polar inversion. They attribute this underestimate to errors in the simulated tidal/gravity wave dissipation, which are potentially coupled to errors in the vertical distribution of aerosols. *Hartogh et al.* [2007], however, do simulate a polar inversion comparable to that observed by *McCleese et al.* [2008], which results from a complex mean meridional circulation in which the PMOC is split into two (or more) branches; one branch upwells strongly at ~15 km above the surface in the northern tropics and downwells at ~50°S, while the other branch upwells strongly at ~50 km above the surface and downwells at the south pole. *Hartogh et al.* [2007] suggest that the lower branch is the classical Hadley circulation and the upper branch is a wave-driven circulation comparable to those in Earth's stratosphere and mesosphere. *Hartogh et al.* [2007] present their results in terms of a residual meridional circulation (“the transformed Eulerian mean”) [*Andrews and McIntyre*, 1976], which has proven more useful for understanding meridional transport of constituents than the conventional Eulerian mean presented in most modeling papers that focus on the Martian general circulation and is related to diabatic heating and cooling within the atmosphere [*Holton*, 2004]. Yet note that since the middle atmospheric aerosol forcing in the simulations of *Hartogh et al.* [2007] is small, the diabatic heating and cooling (mainly through re-radiation by CO₂ of surface emission) implied by the upwelling and downwelling of the upper branch is inherently supported by mechanically driven adiabatic heating and cooling, just as shown in the Eulerian mean analyses of other GCM simulations.

[11] In Earth's atmosphere, an analogous connection between the mean meridional circulation of the troposphere and the mesosphere is generally inhibited by the high stability of the stratosphere. However, certain types of waves, particularly gravity waves, can be transmitted between the troposphere and mesosphere. Interaction between the circulations of the different layers of the atmosphere by means of waves is generally called “dynamic coupling” [e.g., *Miyahara et al.*, 1993]. Simulations such as *Wilson* [1997] and *Hartogh et al.* [2007] and validating observations from instruments such as MCS suggest that coupling between the mean flow of the lower and middle atmosphere is possible on Mars. We will call this phenomenon, “kinematic coupling.”

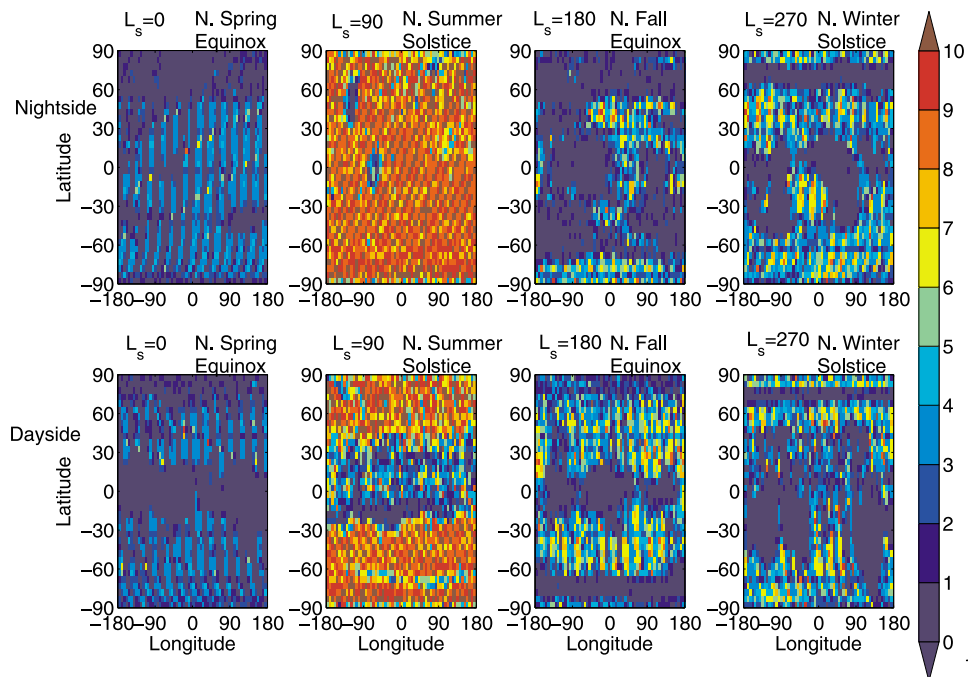


Figure 1. Number of retrievals per latitudinal/longitudinal bin for the labeled time of day and L_s bins during MY 29. The color scale is deepest red for 10 retrievals or more.

[12] In the companion paper, *McCleese et al.* [2010] present the seasonal cycle of the thermal structure and aerosol distribution during Mars Year (MY) 29 (according to the convention of *Clancy et al.* [2000]), a year without a global dust storm. In this study, we treat these observations (within their uncertainties) as partial output from the perfect numerical model (the Martian surface/atmosphere system itself) and use basic theoretical results from atmospheric dynamics and the results of past modeling experiments to infer the “missing” output. Since the MCS retrievals are limited in time-of-day coverage and repeat cycling, we will only use this approach to explore the fundamental characteristics of the mean meridional circulation from the surface to ~ 80 km (10^{-2} – 10^{-3} Pa) and consider the extent to which the mean meridional circulations in the lower and middle atmosphere are kinematically coupled throughout the entire Martian year. In section 6, we briefly consider an alternative approach to the assessment of kinematic coupling.

2. Data

2.1. Retrievals

[13] *McCleese et al.* [2007] describes the MCS instrument and observing strategy. *Kleinböhl et al.* [2009a] describes the first generation retrieval algorithm applied to MCS data. Atmospheric retrievals from MCS observations provide vertical profiles with respect to pressure, p (Pa), of temperature, T (K), dust opacity, i.e., the extinction per unit path length (km^{-1}) due to dust, $d_z\tau_{\text{dust}}$ at 463 cm^{-1} , and water ice opacity, $d_z\tau_{\text{H}_2\text{Oice}}$ (km^{-1}) at 843 cm^{-1} . Pressure is the intrinsic vertical coordinate system for the MCS observations. The retrievals used here were generated using a more advanced retrieval algorithm than described by *Kleinböhl et al.* [2009a], which includes the effects of aerosol scattering in the radia-

tive transfer, as well as nadir and off-nadir observations during most of MY 29. These changes are described in a presentation by *Kleinböhl et al.* [2009b] and by A. Kleinböhl et al. (A single-scattering approximation for infrared radiative transfer in limb geometry in the Martian atmosphere, submitted to *Journal of Quantitative Spectroscopy and Radiative Transfer*, 2011). We also make use of altitude information derived from the geometric pointing of the instrument.

2.2. Zonal Averaging and Sampling

[14] To study the zonal average circulation of the planet, the MCS retrievals and quantities derived from them (as described in later in section 2) during Mars Year (MY) 29 are averaged after being binned by L_s (5° resolution centered at 0° , 5° etc.); time of day: “dayside” (0900–2100 LST) and “nightside” (2100–0900 LST); latitude (5° resolution); and longitude (5.625° resolution). Latitude and longitude refer to the coordinates at the tangent point of the limb path observed by the center of the MCS detector array at ~ 40 km above the surface. Zonal averages are the average of the longitudinal averages in all longitudinal bins containing successful retrievals. All averages were made on pressure coordinates but are plotted against the zonal average (on pressure coordinates) altitude above the areoid of the retrievals, hereafter referred to as the altitude.

[15] Figure 1 plots the population of retrievals in individual latitudinal-longitudinal bins in the L_s bins corresponding to the equinoxes and solstices. The nightside at northern summer solstice is most densely sampled (closest to optimal given ideal operation of the instrument, spacecraft, and retrieval algorithm), while the dayside at northern spring equinox is least densely sampled. Undersampling is usually attributable one of two reasons: (1) operational: the instrument is powered off (as was the case just before northern spring equinox of

MY 29), or the spacecraft is pointed significantly off nadir; and (2) aerosol opacities are high, due to dust storms, or due to tropical water ice clouds during northern spring and summer [Kleinböhl et al., 2009a].

2.3. Winds

[16] An estimate of the zonal gradient wind, $U(p)$, is derived from the zonal average of temperature by taking the lowest pressure level with retrieved temperature data in each latitudinal bin as a level of no motion, p_{LNM} , and estimating the thermal wind, $\hat{U}(p)$:

$$\hat{U}(p) = \int_{p_{LNM}}^p \frac{R_d}{f} \left(\frac{dT}{dy} \right)_p d \ln p' \quad (1)$$

where R_d is the specific gas constant, f is the Coriolis parameter for the latitudinal bin, and $\left(\frac{dT}{dy} \right)_p$ is the temperature gradient at constant pressure. To account for centrifugal force balance and thus compute the gradient wind $U(p)$, we iteratively apply equation (2) to convergence [Holton, 2004]:

$$U_{n+1}(p) = \frac{U_n}{1 + \frac{\sqrt{U_n^2}}{|fR_m|}} \quad (2)$$

where R_M is the radius of Mars. Equations (1) and (2) are only appropriate for winds in approximate geostrophic balance and so cannot be used for diagnosis of zonal winds in the tropics due to the low magnitude of the Coriolis parameter.

2.4. Density-Scaled Opacity

[17] We use the density-scaled opacity as a proxy for aerosol mass mixing ratio. This quantity is the quotient of aerosol opacity and density (computed from the retrieved temperature, pressure, and the ideal gas law). Heavens et al. [2010b] show an example conversion of density-scaled opacity to mass mixing ratio and briefly describe the uncertainties of this conversion.

3. Investigative Approach

3.1. Concerning Zonal Average Plots

[18] Zonal averages of temperature, zonal wind, and aerosol mass mixing ratio are often used in modeling studies [e.g., Richardson and Wilson, 2002] to illustrate aspects of the simulated circulation, particularly the mean meridional circulation. These studies typically report diurnal averages in order to exclude much of the influence of Mars's strong diurnal radiative (hereafter called "thermal") tide on the presentation of the simulated fields. The diurnal variability in the observed fields, however, provides useful insight into issues such as diabatic heating by aerosols and so will be considered here.

[19] In both the real atmosphere and numerical models, zonal average distributions are the result of multiple, often coupled processes with scales ranging from the global to the microscale. In the case of a numerical model, the output can be used both to diagnose the circulation and determine the contributions of particular processes. Likewise, zonal averages of observed data can be used in combination with insights from classical atmospheric dynamical theories primarily

developed for understanding the atmospheric circulation of Earth [e.g., Holton, 2004] and an ensemble of radiative-convective models of the Martian atmosphere [e.g., Colburn et al., 1989; Joshi et al., 1995; Haberle et al., 1997; Zalucha et al., 2010] to develop conceptual models of the mean meridional circulation throughout the lower and middle atmospheres at the equinoxes and solstices. These observationally derived conceptual models can be compared with the output from numerical models to identify aspects of the circulation in the real atmosphere on which modeling experiments should focus. Further improvement of our understanding of the mean meridional circulation eventually may rely upon the assimilation of temperature and aerosol concentrations into a GCM [e.g., Houben, 1999; Lewis et al., 2007; Wilson et al., 2008] or direct measurements of the wind field. The first solution, however, can only be implemented if the dominant processes in the atmosphere are well represented by the baseline numerical simulations used in assimilation.

[20] Since longitudinal sampling by MCS retrievals is minimal in some seasons (Figure 1), the zonal averages presented in this study are not necessarily fully representative of the real zonal mean. Zonal temperature averages based on even a small number of longitudinal bins should be accurate under most conditions: a consequence of the relative weakness of eddies in comparison to planetary-scale circulations like the nonmigrating thermal tides [Zurek et al., 1992]. Dust storm conditions may be an exception. Dust heating aloft may occur faster than the planetary circulation can adjust, while temperatures near the surface are suppressed relative to less dusty areas. Another exception may be the northern hemisphere during the winter, during which baroclinic eddy amplitudes are known to be large [Barnes, 1980, 1981; Wilson et al., 2002], but this region is better sampled longitudinally. The zonal average aerosol distributions should be interpreted cautiously, since they are averages of the dust and water ice distributions over regions with successful retrievals and thus may not include information from areas with high aerosol opacity or unusual aerosol grain size. The high air mass factor of MCS limb observations a priori makes retrieval success unlikely at high aerosol opacities, biasing the zonal averages toward regions/vertical ranges with low dust/ice opacities.

3.2. Qualitative Reconstruction of the Mean Meridional Circulation

[21] We reconstruct the mean meridional circulation qualitatively by making direct inferences from the zonal average plots about upwelling, downwelling, and the strength of meridional and vertical mixing. Those direct inferences are supplemented with insights previously gleaned from theory and modeling to construct conceptual models of the mean meridional circulation appropriate to each season. These conceptual models are necessarily tentative and are intended to motivate future modeling investigations, process-focused analysis of observational data sets, or additional measurements.

[22] Inferring upwelling and downwelling from the thermal structure is primarily an assessment of departure from radiative equilibrium temperatures. As air is forced to rise (sink) in the atmosphere, it will cool (warm) adiabatically. Therefore, in the absence of diabatic heating by absorption of

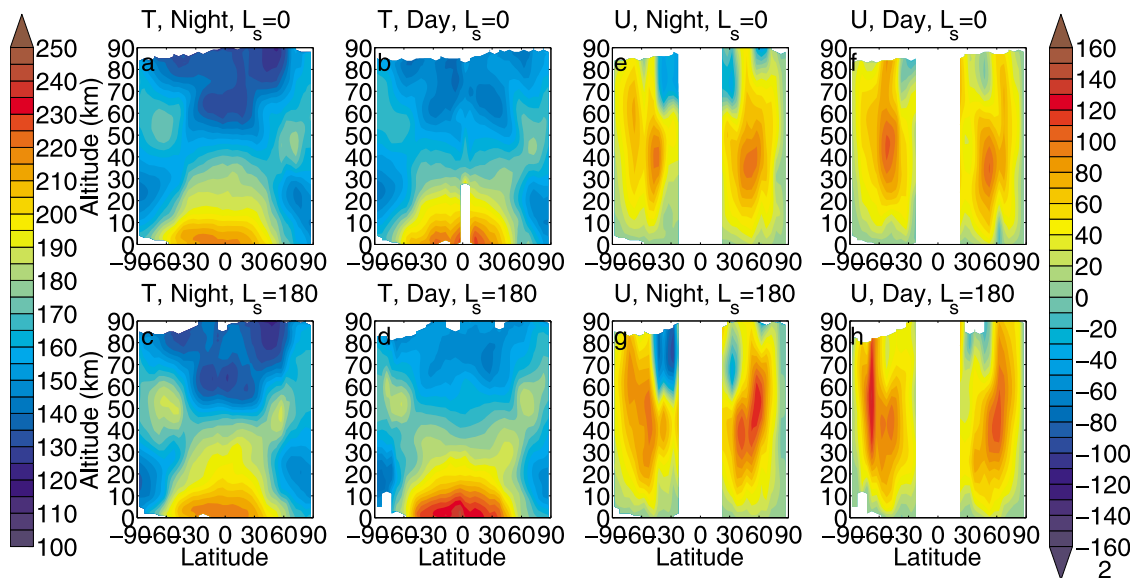


Figure 2. (a–d) Zonal average temperature (K) during MY 29 for the labeled time of day and L_s bins during MY 29. (e–h) Estimated zonal wind velocity (ms^{-1}) for the labeled time of day and L_s bins during MY 29. Contours are every 10 ms^{-1} .

visible and infrared radiation by aerosols or trace gas species (at least those not included in radiative equilibrium models), departure of temperatures from radiative equilibrium directly indicates upwelling and downwelling driven by dynamical processes.

[23] The vertical distribution of dust in Mars’s atmosphere is a measure of the nonsurface radiative forcing of atmospheric circulations on all scales and indicative of the meteorological systems that lift dust. (Studies of dust lifting, transport, and radiative forcing are the subject of future papers; the primary focus here is on the connection between seasonal variability in the dust distribution and seasonal variability in the circulation.) The global atmospheric circulation also redistributes lifted dust, so dust can be a useful tracer of the mean meridional overturning circulation, particularly in the lower atmosphere [Richardson and Wilson, 2002; Kahre et al., 2006]. Characteristic sedimentation velocities are of the same magnitude as characteristic vertical velocities of the planetary-scale circulation, $\sim 10^{-2} \text{ ms}^{-1}$, so when dust is injected into the atmosphere, it will tend to rise or remain stable in zones of mean upwelling but sink more quickly by its own negative buoyancy in combination with the large-scale flow in zones of mean downwelling. Sedimentation of Martian dust is sufficiently slow that it can be advected thousands of kilometers from where it is lifted [Murphy et al., 1993], making dust a tracer of both horizontal and vertical flows on time scales shorter than its atmospheric residence time. This method of inference is, however, complicated by the dependence of the sedimentation velocity on air density and particle size. The sedimentation velocity increases with height, and so dust may not be fully distributed through a region of positive vertical velocity. Other complications include the potential removal or obscuration of dust by condensation of water ice or carbon dioxide ice.

[24] The vertical distribution of water ice in the atmosphere constrains the vertical profile of water vapor and radiative forcing by water ice. Water ice also can be a tracer of moist

air at temperatures sufficiently cold for saturation, and the path of water vapor from its sources (mainly warming water ice caps at the poles or subsurface ice deposits at high latitudes), which is controlled in part by the mean meridional circulation. In the simulations of Richardson et al. [2002], a water ice maximum over the northern tropics originates from water vapor coming from the northern pole during summer near the surface, which then strongly upwells into colder atmosphere at $\sim 150 \text{ Pa}$. Following this result, we will infer that an area with high concentrations of water ice spanning a strong vertical temperature gradient is a zone of upwelling. Such an inference can be complicated by variations in available condensation nuclei and advection, diffusion, and sedimentation of water ice. Hinson and Wilson [2004] and Lee et al. [2009], however, point out that if there is tidal control of the water ice distribution, the effects of advection, diffusion, and sedimentation can be mostly neglected.

4. Equinoxes

4.1. Description

[25] The thermal structure at northern spring equinox (Figures 2a–2b) is effectively mirror symmetric about the equator. The principal exceptions to this symmetry are the temperature minima near the poles. (We call these minima “polar vortices,” though vorticity is not diagnosed here, because modeling and observations of aeolian features suggest they correspond to circulations similar to Earth’s polar vortices [e.g., French and Gierasch, 1979].) The winter-leaving north polar vortex extends from the remnant cold surface to $\sim 35 \text{ km}$. The surface and lower atmosphere are warmer in the south, and so confine the southern polar vortex to a narrower altitude range. At northern fall equinox (Figures 2c–2d), the thermal structure is very similar to the northern spring equinox, except that the high latitudes at $\sim 50 \text{ km}$ and the tropics at $\sim 30 \text{ km}$ are warmer. The estimated zonal wind distribution at both equinoxes consists of two

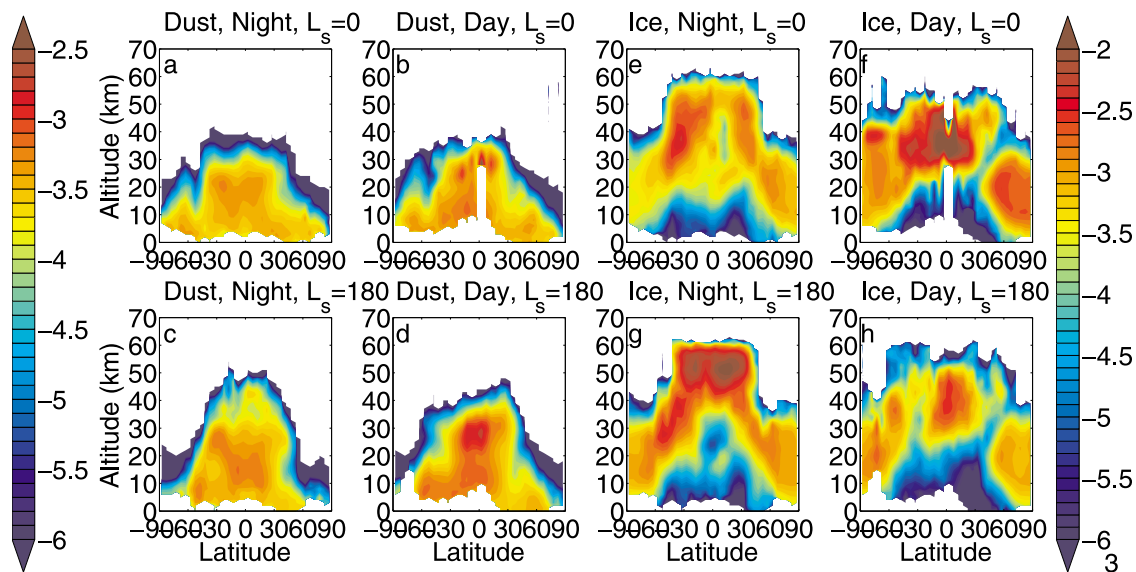


Figure 3. (a–d) Log_{10} of the zonal average dust density-scaled opacity ($\text{m}^2 \text{kg}^{-1}$) for the labeled time of day and L_s bins during MY 29. (e–h) Log_{10} of the zonal average water ice density-scaled opacity ($\text{m}^2 \text{kg}^{-1}$) for the labeled time of day and L_s bins during MY 29. Contours are every 0.1 log units.

zonal jets in the midlatitudes. At northern spring equinox, the maxima of these jets are centered at 35–45 km (Figures 2e–2f). These maxima are somewhat higher in magnitude and broader in vertical extent at northern fall equinox (Figures 2g–2h).

[26] The dust distributions at both equinoxes are relatively symmetric about the equator. Dust density-scaled opacity is higher and dust penetrates to higher altitudes near the equator (Figures 3a–3d) than at the poles. Dust density-scaled opacity also appears to be higher in the tropical atmosphere at northern fall equinox than at northern spring equinox.

[27] The water ice distributions at both equinoxes differ between day and night due to the influence of the thermal tides [Lee *et al.*, 2009]. The clearest difference appears on the nightside, where the layer of water ice on the tropics between 45 km and 60 km is up to an order of magnitude higher in density-scaled opacity at northern fall equinox than northern spring equinox (Figures 3e and 3g). On the dayside, the layer of water ice on the tropics at ~35 km is higher in density-scaled opacity at northern spring equinox than northern fall equinox (Figures 3f and 3h). Thus, while there are some second-order differences, the thermal structure and aerosol distributions at both equinoxes are sufficiently similar that their qualitative mean meridional circulations will be effectively interchangeable.

4.2. Diagnosis of Upwelling and Downwelling

[28] Figures 4a–4c replot zonal average nightside temperature (Figure 2a), dust density-scaled opacity (Figure 3a), and water ice density-scaled opacity (Figure 3e) for northern spring equinox with upward and downward (solid for definite, dashed for ambiguous) arrows to indicate zones of upwelling and downwelling inferred from the zonal average fields. At the equinox, temperature maxima of the polar warmings are ~170 K, and from the ensemble of models we see that this temperature is at least 35 K above radiative equilibrium temperatures. Importantly, ice and dust are

largely absent from the latitudes and altitudes corresponding to the warmings, and the magnitudes of the temperature maxima are fairly similar between the dayside and nightside, thus eliminating the possibility that diabatic heating of aerosol is driving the strong departure from radiative equilibrium. Instead, dynamically driven downwelling is indicated.

[29] Nightside temperatures at ~55 km in the tropics are ~130 K and dayside temperatures are ~150 K, a variation likely driven by the tides [Lee *et al.*, 2009]. The average temperature is thus at least 10 K below radiative equilibrium. Water ice is present at the lower end of this zone of very cold temperatures, but water ice will absorb infrared radiation from below, re-emit it at a lower temperature, and produce a net diabatic heating. Thus, the presence of water ice cannot explain why temperatures are cooled below radiative equilibrium. Thus, adiabatic cooling and upwelling are diagnosed.

[30] Dust density-scaled opacities at 10 km are relatively similar from pole to pole, but the vertical extent of dust is significantly deeper from 40°S to 25°N, indicating strong vertical and meridional mixing in the lower atmosphere at these latitudes. There is a minimum in dust density-scaled opacity at ~50°S at 20 km. We infer that this minimum is probably due to downwelling. Scavenging by water is less likely since ice density-scaled opacities at this latitude and level are relatively similar to those at higher latitudes, where the vertical extent of dust is deeper.

[31] High ice density-scaled opacities are observed over a broad vertical range centered at ~40 km at between 45°S and 45°N, which is a region with a negative vertical temperature gradient. We infer broad upwelling at this level and region.

[32] The upwelling and downwelling zones identified here are consistent with meridional cells symmetric about the equator in both the lower and middle atmospheres that rise at the equator and sink at higher latitudes. In the lower atmosphere, the average insolation is strongest at the equator, so

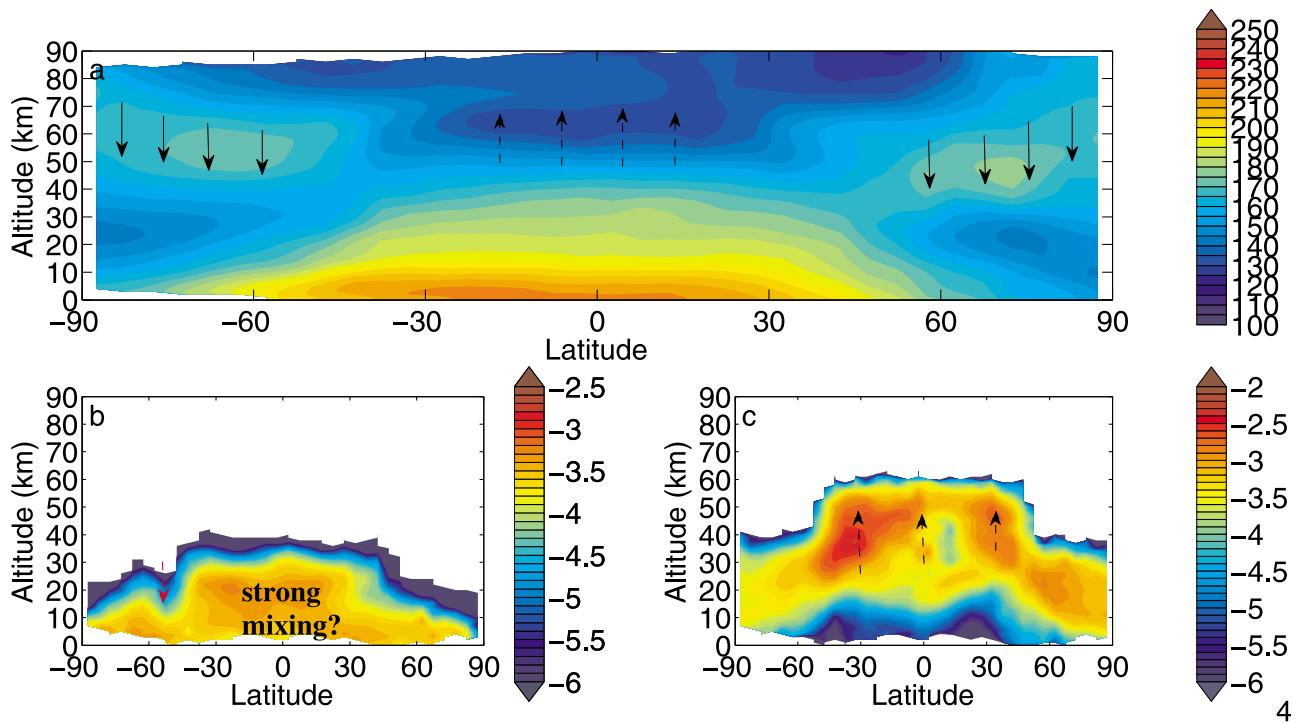


Figure 4. Characteristic zonal average fields for an equinoctial case ($L_s = 0^\circ$, nightside) with inferred zones of upwelling (upward arrows), downwelling (downward arrows), and vigorous mixing (label) indicated. Definite inferences are marked with solid arrows. More ambiguous inferences are marked with dashed arrows. The color of arrows is for sake of clarity and has no other significance: (a) Temperature (K), identical to Figure 2a; (b) dust density-scaled opacity ($\text{m}^2 \text{kg}^{-1}$), identical to Figure 3a; (c) water ice density-scaled opacity ($\text{m}^2 \text{kg}^{-1}$), identical to Figure 3e.

the differential heating between the equator and pole creates an unstable flow regime due to incompatibility between radiative equilibrium and angular momentum conservation. To resolve this instability, equatorial air rises from the surface and moves poleward. This air cools at higher latitudes, sinks, and becomes a return flow back to the equator, forming two meridional circulation cells symmetric about the equator: the PMOCs. In the middle atmosphere, theory and modeling suggest that similar cells can be driven by dissipation of waves and tides or aerosol diabatic forcing [e.g., *Holton et al.*,

1995; *Forget et al.*, 1999; *Forbes and Miyahara*, 2006; *Hartogh et al.*, 2007; *Wilson et al.*, 2008].

[33] In order to draw a full set of streamlines for the circulation, it is necessary to know to what extent the lower and middle atmospheric meridional cells are coupled kinematically, but the observations leave that question ambiguous. Different possible scenarios consistent with the inferred upwelling and downwelling are illustrated schematically on the same temperature plot as Figure 4a in Figure 5. The lower and middle atmospheric meridional cells may be separated by

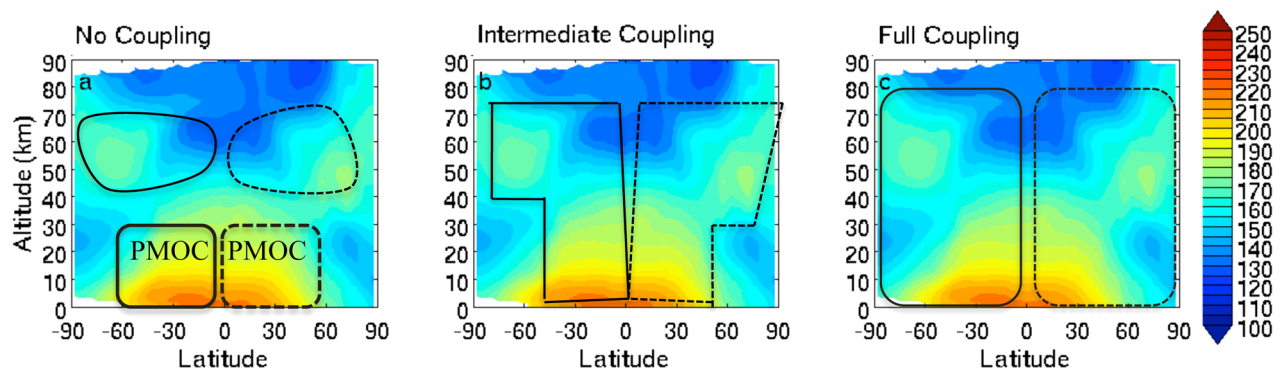


Figure 5. Characteristic temperature fields for the equinoctial case: (a–c) as in Figure 4 marked with schematic streamlines of the inferred mean meridional circulation for three possible states of coupling as labeled. The solid streamlines indicate counterclockwise flow, and the dashed streamlines indicate clockwise flow.

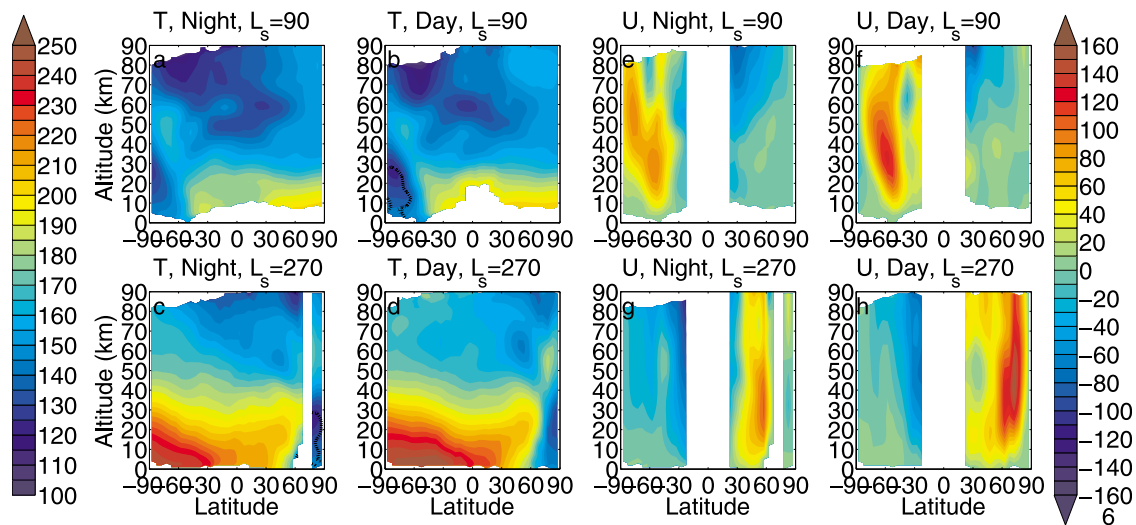


Figure 6. (a–d) Zonal average temperature (K) during MY 29 for the labeled time of day and L_s bins during MY 29. (e–h) Estimated zonal wind velocity (ms^{-1}) for the labeled time of day and L_s bins during MY 29. Contours are every 10 ms^{-1} .

a region of weak vertical motion (opposite to the mutual upwelling or downwelling in the cells) (Figure 5a) and thus be fully decoupled kinematically. The lower and middle atmospheric cells in one hemisphere may be fully kinematically coupled in a single cell, in which air rises at the equator into the middle atmosphere, strongly descends within the middle atmospheric polar warming to the surface (Figure 5c). In the latter case, there would be substantial mixing of constituents both meridionally and vertically. In the former case, mixing would be primarily meridional, isolating the lower from the middle atmosphere with implications for the atmospheric loss of water vapor and other constituents. We note that a Mars GCM simulation of this season by *Forget et al.* [1999] suggests the local temperature maxima of the polar warmings are consistent with an intermediate state of coupling (Figure 5b), in which the PMOC extends deeply into the middle atmosphere in the tropics, is pulled poleward more strongly in the middle atmosphere than in the lower atmosphere by the forcing of the middle atmospheric meridional cell, and returns in the middle atmosphere to merge with the downwelling of the deep tropical PMOC at midlatitudes. Thus, the PMOC in this simulation is kinematically coupled with the mean meridional cell in the middle atmosphere in the tropics but not at higher latitudes.

5. Solstices

5.1. Description

[34] The thermal structure and aerosol distributions differ significantly between the northern summer and the northern winter solstices of MY 29. Temperatures throughout the atmosphere (except in the polar vortex) are considerably warmer at northern winter solstice than northern summer solstice (Figures 6a–6d). In the lower atmosphere (altitudes less than 35 km) at northern winter solstice, temperatures are usually highest in the southern high latitudes, lower toward the tropics, and have a secondary maximum in the northern midlatitudes that tilts poleward at lower pressures. This qualitative thermal structure is only weakly apparent at

northern summer solstice. In the middle atmosphere, there is a temperature maximum at 35–70 km near the winter pole at both solstices, which is slightly warmer and centered at higher altitude at northern winter solstice. The estimated zonal wind structures are qualitatively similar at both solstices and consist of a strong westerly jet (stronger at northern winter solstice) in the middle and high latitudes of the winter hemisphere and weak westerlies or easterlies in the middle and high latitudes of the summer hemisphere (Figures 6e–6h).

[35] At both solstices, dust is primarily restricted to the summer hemisphere and winter hemisphere tropics (Figures 7a–7d). A region of extremely dust clear air generally separates the dust in the winter tropics from aerosol in the winter high latitudes (likely CO_2 ice retrieved here as dust). This region of dust clear air is broader at northern summer solstice. In the winter tropics and summer hemisphere, dust density-scaled opacity is higher at northern summer solstice. As discussed by *McCleese et al.* [2010], the summer hemisphere and tropical dust distributions at northern summer and northern winter solstice also differ in stratification. Dust density-scaled opacity is constant or decreases with height at northern winter solstice but tends to increase with height in the tropics below 20 km at northern summer solstice.

[36] The water ice distributions at the solstices differ significantly (Figures 7e–7h). The northern summer solstice distribution is dominated by a high density-scaled opacity layer of water ice in the northern tropics at ~ 30 km, but smaller amounts of water ice are present at all latitudes at altitudes less than 40 km. At northern winter solstice, the thickest layers of water ice are restricted to the summer hemisphere at altitudes greater than 40 km. Note that water ice density-scaled opacity is higher in the winter polar vortex at northern winter solstice.

[37] Due to differing topography and summer insolation between the northern and southern hemispheres (and seasonal variability in dust loading and distribution), the southern summer solstitial circulation (at least the PMOC) is believed to be more vigorous than its northern analog [*Zurek et al.*, 1992; *Richardson and Wilson*, 2002; *Takahashi et al.*,

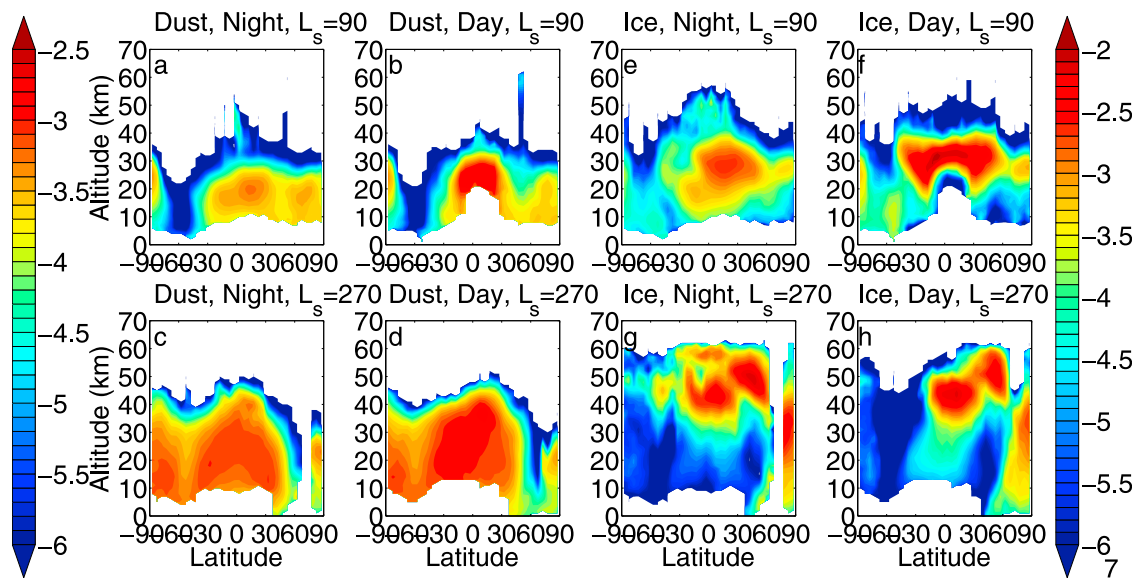


Figure 7. (a–d) Log_{10} of the zonal average dust density-scaled opacity ($\text{m}^2 \text{kg}^{-1}$) for the labeled time of day and L_s bins during MY 29. (e–h) Log_{10} of the zonal average water ice density-scaled opacity ($\text{m}^2 \text{kg}^{-1}$) for the labeled time of day and L_s bins during MY 29. Contours are every 0.1 log units.

2003]. We will diagnose the circulations at the solstices separately.

5.2. Diagnosis of Upwelling and Downwelling

[38] Figures 8a–8c replot zonal average dayside temperature (Figure 6d), dust density-scaled opacity (Figure 7d), and water ice density-scaled opacity (Figure 7h) for southern summer solstice with arrows indicating upwelling and down-

welling as in Figures 4a–4c. The temperature of the middle atmospheric polar warming near the north pole is ~ 180 K. The temperature of this warming exceeds temperatures at this level at all other latitudes on both the dayside and nightside (Figure 6c), so it can be inferred to be much warmer than radiative equilibrium. Comparison with the ensemble of models, [see *Haberle et al.*, 1997] suggests the departure from radiative equilibrium of the observed warming is at least

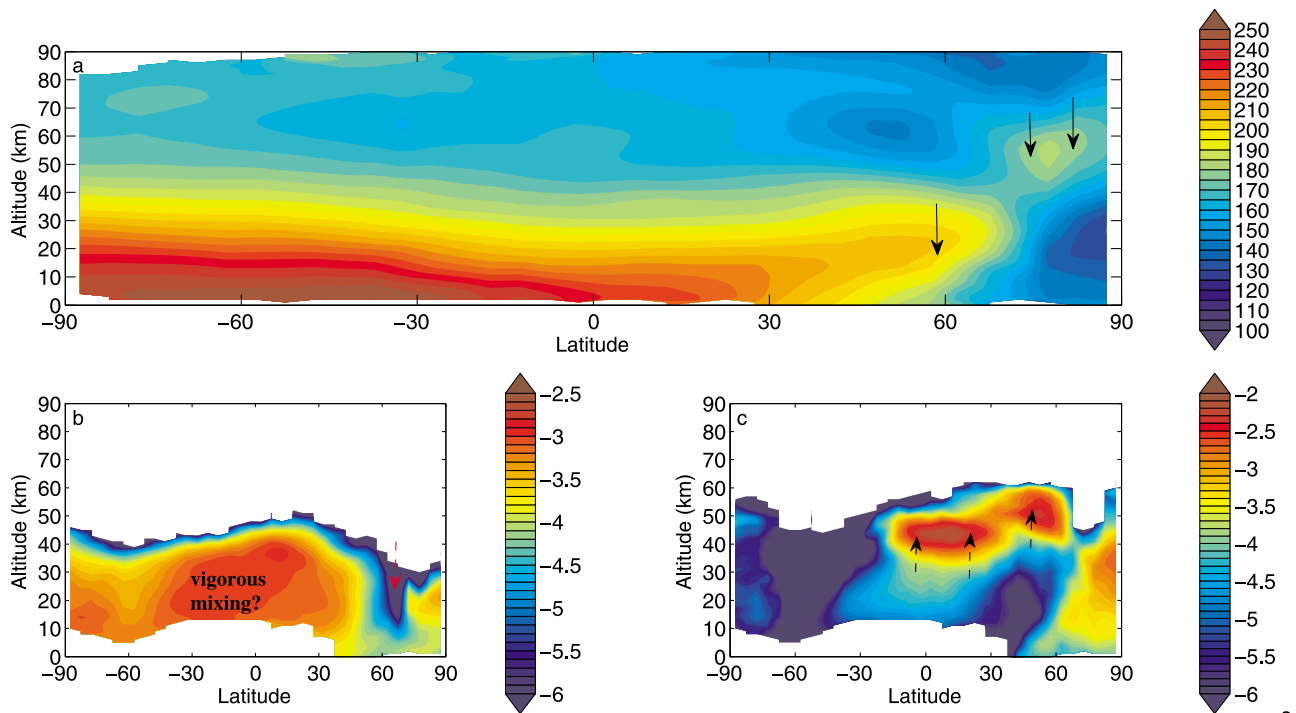


Figure 8. As Figure 4 except for the northern winter solstice ($L_s = 270^\circ$, dayside).

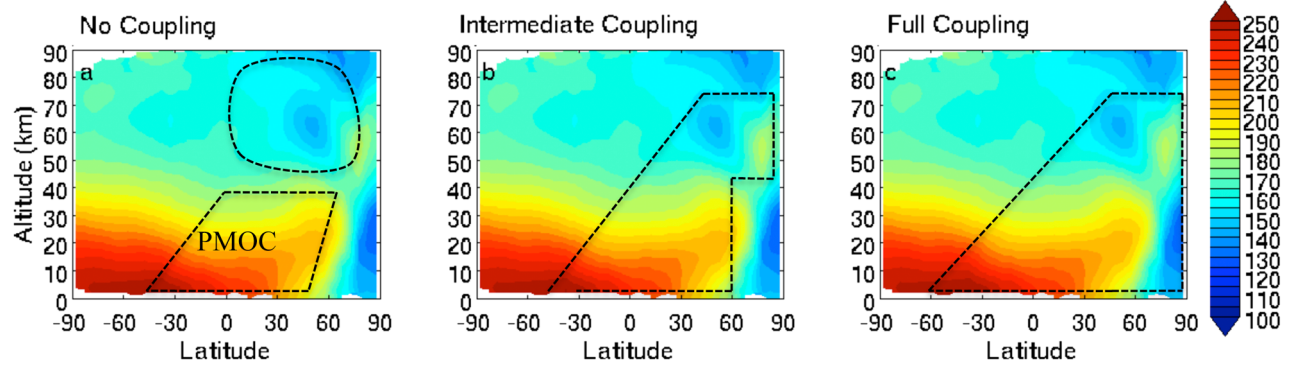


Figure 9. As Figure 5 except for the northern winter solstice.

70 K. The warming is at latitudes with no or limited solar insolation at this season, so downwelling is inferred. In the lower atmosphere, there is a substantial temperature inversion centered at 25 km and 60°N. Comparison with *Haberle et al.* [1997] suggests that the departure from radiative equilibrium of the observed warming is at least 50 K. This region is mostly free of water ice and dust, which suggests diabatic heating is minimal, so downwelling is inferred. Between 30°S and 10°N at 30–50 km altitude, there is a temperature minimum. High concentrations of dust and water ice are present at the lower and upper and northern ends of this region, respectively. While it is possible that the combined shortwave heating of dust, longwave heating of water ice, and proximity to the subsolar point should support a temperature maximum in this region in the absence of adiabatic heating/cooling, comparison of the temperatures here with the model of *Haberle et al.* [1997] suggests that they are within 10 K of radiative equilibrium, so upwelling is not diagnosed here.

[39] Dust density-scaled opacities are high and roughly constant with pressure at pressures greater than 20 Pa from 40° to 30°N, indicating strong vertical and meridional mixing in the lower atmosphere at these latitudes. There is a minimum in dust concentrations at ~60°N and 20 km. Water ice concentrations at this latitude and level are higher than at lower latitudes, so this minimum could be due to scavenging or downwelling.

[40] The upwelling and downwelling zones identified here are consistent with single meridional cells in the lower and the middle atmospheres. The lower atmosphere cell (the PMOC) rises in the southern midlatitudes and sinks at 60°N. The theory of *Lindzen and Hou* [1988] suggests the latitude of PMOC downwelling corresponds to the latitude of upwelling in the opposite hemisphere, but there is no definite confirmation of this idea from the observations. In the middle atmosphere, the downwelling near the pole indicates a middle atmospheric cell, but it is unclear from the observations whether the upwelling of this cell takes the form of weak upwelling in the middle atmosphere from the summer pole to the winter midlatitudes or stronger, more localized upwelling.

[41] Figure 9 shows schematically three possible structures of the mean meridional cells for different states of kinematic coupling. The discontinuity between the warming due to downwelling in the lower atmosphere near 60°N and the warming due to downwelling in the middle atmosphere near the north pole suggests that the PMOC in the lower atmo-

sphere is not fully kinematically coupled with the meridional cell in the middle atmosphere. The polar warming in a simulation of the circulation in this season by *Forget et al.* [1999] is 50 K warmer than the observed polar warming. In this simulation, the meridional mass stream function is consistent with nearly complete coupling between the PMOC and the mean meridional cell in the middle atmosphere, since the streamlines of the PMOC in the northern high latitudes remain vertical as low as 15 km above the surface (as opposed to 55 km in the equinoctial case). Because of the similarity between the temperature of the polar warming simulated by *Forget et al.* [1999] and observed dust storm polar warmings, it is possible that dust storm polar warmings are the result of a fully kinematically coupled lower and middle atmospheric meridional circulation. In other words, the “pole-to-pole” circulation in the simulations of *Wilson* [1997], *Forget et al.* [1999], and *Kuroda et al.* [2009] is a fully kinematically coupled lower and middle atmospheric meridional circulation. From the observations alone, we cannot infer anything about the vertical structure of tropical upwelling. So we cannot determine from this analysis whether the lower and middle atmospheric meridional cells are in an intermediate state of coupling or fully decoupled.

[42] The dust clear air in the winter high latitudes at ~20 km is consistent with the area of the atmosphere heated primarily by downwelling in the lower atmospheric PMOC. On the poleward side of the vortex wall, water ice opacities increase again [*Benson et al.*, 2010], but density-scaled opacities are much lower than in the tropical cloud belt. The southern winter atmosphere is seen to be much clearer of ice than the northern winter atmosphere, consistent with Mars Odyssey Gamma Ray Spectrometer argon observations [*Sprague et al.*, 2007] that suggest that the southern polar vortex is much more dynamically isolated than the northern one.

[43] Figures 10a–10c replot zonal average nighttime temperature (Figure 6a), dust density-scaled opacity (Figure 7a), and water ice density-scaled opacity (Figure 7e) for northern summer solstice with arrows indicating upwelling and downwelling as in Figures 4a–4c and 8a–8c. The temperature of the middle atmospheric polar warming near the south pole is ~170 K (Figure 10a). Because the temperature of this warming on the nightside or dayside (Figure 6b) exceeds temperatures at this level at all other latitudes, it can be inferred to be much warmer than radiative equilibrium. The ensemble of radiative-convective models (particularly *Zalucha*

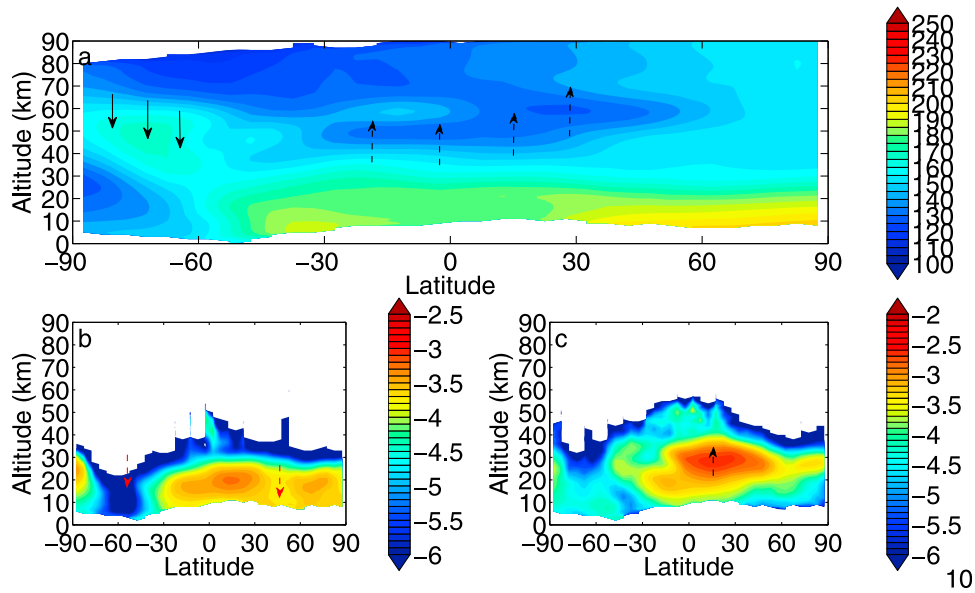


Figure 10. As Figure 4 except for the northern summer solstice ($L_s = 90^\circ$, nightside).

et al. [2010]) suggests temperatures exceed radiative equilibrium by at least 35 K, so downwelling is inferred. Temperatures at ~50 km in the tropics average ~135 K. The average temperature is at least 20 K below radiative equilibrium [Colburn *et al.*, 1989], so upwelling is inferred there.

[44] Downwelling is inferred in the vicinity of the region of dust clear air centered at 60°S and ~15 km (Figure 10b), where there is a maximum in temperature and a minimum in water ice, possibly indicating a region of adiabatic warming. Dust density-scaled opacity has a notable minimum at ~45°N and ~15 km altitude. Since water ice density-scaled opacity at this pressure level is higher in the southern tropics than in this region, enhanced scavenging by water ice is not a convincing explanation for the minimum, so downwelling is inferred there.

[45] Water ice concentrations are highest at ~30 km over the northern tropics (Figure 10c). Temperatures are decreasing with altitude at this pressure level. If we interpret this feature as due to a gradual drying of vapor-rich air from the summer pole upwelling across the equator, we may infer broad upwelling throughout this latitudinal band.

[46] Thus, the inferred circulation in the lower atmosphere consists of two PMOCs that upwell in the northern tropics: a stronger, broader cell that downwells in the southern mid-latitudes and a weaker, narrower cell that sinks in the northern midlatitudes. In the middle atmosphere, another cell likely upwells through the tropics and downwells near the winter pole. As at southern summer solstice, observations argue against full kinematic coupling, but the exact degree of kinematic coupling cannot be determined. Possible options are shown schematically in Figure 11.

6. An Alternative Approach to the Analysis of Kinematic Coupling

[47] This study has focused on qualitative and geometric reconstruction of the mean meridional circulation of Mars’s atmosphere. Our implicit assumption has been that the relation between kinematic coupling and temperature departure from radiative equilibrium is purely geometric. Air upwells at low latitudes, converges as it moves toward high latitudes, and downwells more intensely at high latitudes to conserve

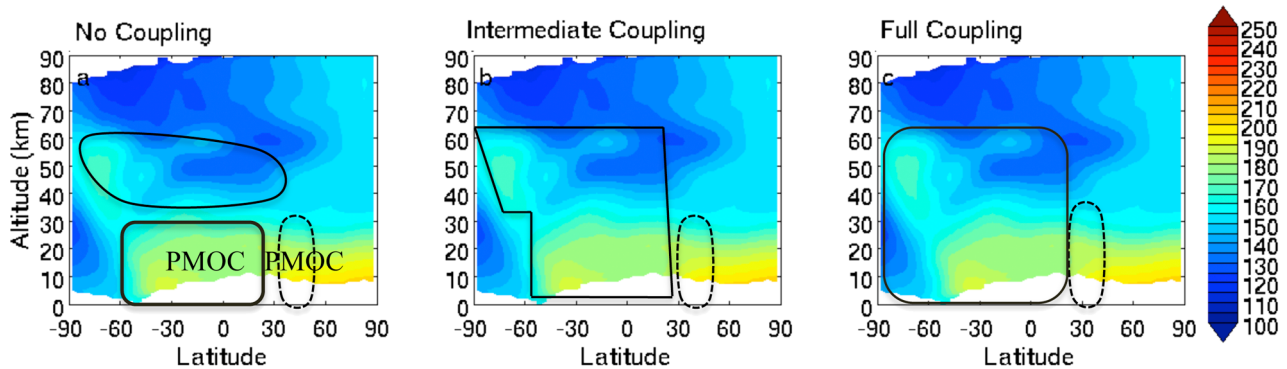


Figure 11. As Figure 5 except for the northern summer solstice.

mass, resulting in adiabatic warming. This framework lacks a ready explanation for why fully kinematically coupled circulations produce much higher-temperature polar inversions than more weakly coupled circulations. One possibility is that this effect is thermodynamic.

[48] As noted by *Wallace and Hobbs* [1976], planetary atmospheres act like heat engines “in a gross, statistical sense,” in which energy is concentrated by solar absorption in the lower atmosphere of the tropics and summer hemisphere and redistributed by circulations like the PMOC toward cooler air at higher altitudes and latitudes. Thus, the generation of mechanical energy to maintain atmospheric circulations depends on the positive thermodynamic efficiency of the atmospheric heat engine implied by this general effective diffusion of heat.

[49] Thus, complete kinematic decoupling of the lower and middle atmospheric mean meridional circulations is unlikely to produce a middle atmosphere in which the equator is substantially cooler than the pole, no matter the intensity of downwelling in the middle atmosphere. A fully isolated middle atmospheric cell would be a thermally indirect circulation equivalent to a heat engine running strongly in reverse. The negative efficiency at the northern summer solstice would be $\sim 25\%$. Such a circulation would need to be sustained entirely by dissipative heating by waves and tides propagating into the middle atmosphere from below, since waves and tides are ultimately driven by diabatic heating in the lower atmosphere. Generously assuming that the gravity waves in Mars’s atmosphere have periods comparable to gravity waves in the Earth’s atmosphere generated by convective updrafts, recent analysis by *Heavens et al.* [2010a] suggests that zonal average direct heating by gravity wave dissipation at an altitude of 10 km above the polar inversions is $\sim 5 \text{ K sol}^{-1}$, except perhaps just before the global dust storm in 2007. Unless dissipative heating by tides or other types of waves is substantially larger, the equator to pole temperature gradient must be sustained by effective eddy diffusion of heat from the tropical lower atmosphere. In that case, the lower and middle atmospheric mean meridional circulations must be at least partially kinematically coupled throughout the year in order to sustain the observed thermal inversions. Such a thermodynamic constraint on similar inversions in the Earth’s mesosphere was recognized by *Leovy* [1964], who noted, “... a counter-gradient heat transport by the mean meridional circulation arises from the fact that the motions in the upper mesosphere are driven by the heat sources at the lower levels.” Thus, the excess radiation of the polar inversions (inside or outside dust storms) should ultimately be a function of the diabatic heating input and the thermodynamic efficiency of the PMOC. It is possible that the latter parameter is related to the geometric description of kinematic coupling used in this study. Testing this hypothesis is beyond the scope of this work but is certainly possible. A technique for estimating the thermodynamic efficiency of simulated circulations has been outlined by *Adams and Rennó* [2005], though their approach may need adjustment to account for the radiative effects of aerosol.

7. Summary

[50] We have used the first simultaneous and systematic observations of the thermal structure and aerosol distributions

of the lower and middle Martian atmosphere to 80 km above the surface to perform a simple, qualitative analysis of the background seasonal variability of the mean meridional circulation. We find that there are vigorous and clearly delineated middle atmospheric cells at all seasons of the year. These cells are associated with strong positive equator-pole gradients in temperature, so they are thermodynamically implausible unless they are at least partially “kinematically” coupled to the PMOC in the lower atmosphere. Yet in all cases during the year analyzed, the coupling appears to be much weaker than indicated by GCM simulations of dust storm polar warmings, underlining the exceptional nature of these events. Therefore, the most plausible coupling scenario is one in which the tropical upwelling of the principal lower and middle atmospheric cells is approximately continuous but the downwelling of these cells at higher latitudes is discontinuous. The qualitative analysis presented in this study, however, is tentative and its limitations underline the need for quantitative metrics of kinematic coupling for analysis of both model simulations and observations. Past modeling experiments suggest that kinematic coupling is strongly dependent on the details of the aerosol forcing in the lower atmosphere and the wave forcing in the middle atmosphere, which are being investigated by MCS and The Compact Reconnaissance Imaging Spectrometer for Mars (CRISM) on MRO and will be investigated by the instrument package on the upcoming 2016 ExoMars Orbiter.

[51] **Acknowledgments.** We thank two anonymous reviewers for their helpful comments on this manuscript. We would also like to thank Tina Pavlicek for her contributions to MCS instrument operations and Mark Apolinski for his work on processing the MCS data. We also wish to thank Wayne Hartford and Mark Foote for their contributions to the design and fabrication of the instrument and the MRO spacecraft operations teams who make this investigation possible. This work was performed in part at and funded by the Jet Propulsion Laboratory, California Institute of Technology, under a contract with NASA.

References

- Adams, D. K., and N. Rennó (2005), Thermodynamic efficiencies of an idealized global model, *Clim. Dyn.*, *25*, 801–813, doi:10.1007/s00382-005-0071-y.
- Andrews, D. G., and M. E. McIntyre (1976), Planetary waves in horizontal and vertical shear: The generalized Eliassen-Palm relation and the zonal mean acceleration, *J. Atmos. Sci.*, *33*, 2031–2048, doi:10.1175/1520-0469(1976)033<2031:PWIHAV>2.0.CO;2.
- Angelats i Coll, M., F. Forget, M. A. López-Valverde, and F. González-Galindo (2005), The first Mars thermospheric general circulation model: The Martian atmosphere from the ground to 240 km, *Geophys. Res. Lett.*, *32*, L04201, doi:10.1029/2004GL021368.
- Barnes, J. R. (1980), Time spectral analysis of midlatitude disturbances in the Martian atmosphere, *J. Atmos. Sci.*, *37*, 2002–2015, doi:10.1175/1520-0469(1980)037<2002:TSAOMD>2.0.CO;2.
- Barnes, J. R. (1981), Midlatitude disturbances in the Martian atmosphere: A second Mars year, *J. Atmos. Sci.*, *38*, 225–234, doi:10.1175/1520-0469(1981)038<0225:MDITMA>2.0.CO;2.
- Barnes, J. R. (1991), A simple nearly analytic model of a gravity wave driven middle atmospheric circulation, *J. Atmos. Sci.*, *48*, 225–235, doi:10.1175/1520-0469(1991)048<0225:ASNAMO>2.0.CO;2.
- Benson, J. L., D. M. Kass, A. Kleinbohl, D. J. McCleese, J. T. Schofield, and F. W. Taylor (2010), Mars’ south polar hood as observed by the Mars Climate Sounder, *J. Geophys. Res.*, *115*, E12015, doi:10.1029/2009JE003554.
- Bougher, S. W., G. M. Keating, R. Zurek, J. Murphy, R. Haberle, J. Hollingsworth, and R. T. Clancy (1999), Mars Global Surveyor aerobraking: Atmospheric trends and model interpretation, *Adv. Space Res.*, *23*(11), 1887–1897, doi:10.1016/S0273-1177(99)00272-0.
- Clancy, R. T., B. J. Sandor, M. J. Wolff, P. R. Christensen, M. D. Smith, J. C. Pearl, B. J. Conrath, and R. J. Wilson (2000), An intercomparison of

- ground-based millimeter, MGS TES, and Viking atmospheric temperature measurements: Seasonal and interannual variability of temperatures and dust loading in the global Mars atmosphere, *J. Geophys. Res.*, *105*, 9553–9571, doi:10.1029/1999JE001089.
- Colburn, D. S., J. B. Pollack, and R. M. Haberle (1989), Diurnal variations in optical depth at Mars, *Icarus*, *79*, 159–189, doi:10.1016/0019-1035(89)90114-0.
- Deming, D., M. J. Mumma, F. Espenak, T. Kostiuk, and D. Zipoy (1986), Polar warming in the middle atmosphere of Mars, *Icarus*, *66*, 366–379, doi:10.1016/0019-1035(86)90165-X.
- Forbes, J. M., and S. Miyahara (2006), Solar semidiurnal tide in the dusty Mars atmosphere, *J. Atmos. Sci.*, *63*, 1798–1817, doi:10.1175/JAS3718.1.
- Forget, F., F. Hourdin, R. Fournier, C. Hourdin, O. Talagrand, M. Collins, S. R. Lewis, P. L. Read, and J.-P. Huot (1999), Improved general circulation models of the Martian atmosphere from the surface to above 80 km, *J. Geophys. Res.*, *104*, 24,155–24,175, doi:10.1029/1999JE001025.
- Forget, F., F. Montmessin, J.-L. Bertaux, F. González-Galindo, S. Lebonnois, E. Quémerais, A. Reberac, E. Dimarellis, and M. A. López-Valverde (2009), Density and temperatures of the upper Martian atmosphere measured by stellar occultations with Mars Express SPICAM, *J. Geophys. Res.*, *114*, E01004, doi:10.1029/2008JE003086.
- French, R. G., and P. J. Gierasch (1979), The Martian polar vortex: Theory of seasonal variation and observations of Eolian features, *J. Geophys. Res.*, *84*, 4634–4642, doi:10.1029/JB084iB09p04634.
- Haberle, R. M., C. B. Leovy, and J. M. Pollack (1982), Some effects of global dust storms on the atmospheric circulation of Mars, *Icarus*, *50*, 322–367, doi:10.1016/0019-1035(82)90129-4.
- Haberle, R. M., J. B. Pollack, J. R. Barnes, R. W. Zurek, C. B. Leovy, J. R. Murphy, J. Schaeffer, and H. Lee (1993), Mars atmospheric dynamics as simulated by the NASA/Ames general circulation model: 1. The zonal mean circulation, *J. Geophys. Res.*, *98*, 3093–3123, doi:10.1029/92JE02946.
- Haberle, R. M., H. Houben, J. R. Barnes, and R. E. Young (1997), A simplified three-dimensional model for Martian climate studies, *J. Geophys. Res.*, *102*, 9051–9067, doi:10.1029/97JE00383.
- Hartogh, P., A. S. Medvedev, T. Kuroda, R. Saito, G. Villanueva, A. G. Feofilov, A. A. Kutepov, and U. Berger (2005), Description and climatology of a new general circulation model of the Martian atmosphere, *J. Geophys. Res.*, *110*, E11008, doi:10.1029/2005JE002498.
- Hartogh, P., A. S. Medvedev, and C. Jarchow (2007), Middle atmosphere polar warmings on Mars: Simulations and study on the validation with sub-millimeter observations, *Planet. Space Sci.*, *55*(9), 1103–1112, doi:10.1016/j.pss.2006.11.018.
- Heavens, N. G., M. I. Richardson, W. G. Lawson, C. Lee, D. J. McCleese, D. M. Kass, A. Kleinböhl, J. T. Schofield, W. A. Abdou, and J. H. Shirley (2010a), Convective instability in the Martian middle atmosphere, *Icarus*, *208*, 574–589, doi:10.1016/j.icarus.2010.03.023.
- Heavens, N. G., J. L. Benson, D. M. Kass, A. Kleinböhl, W. A. Abdou, D. J. McCleese, M. I. Richardson, J. T. Schofield, J. H. Shirley, and P. M. Wolkenberg (2010b), Water ice clouds over the Martian tropics during northern summer, *Geophys. Res. Lett.*, *37*, L18202, doi:10.1029/2010GL044610.
- Hinson, D. P., and R. J. Wilson (2004), Temperature inversions, thermal tides, and water ice clouds in the Martian tropics, *J. Geophys. Res.*, *109*, E01002, doi:10.1029/2003JE002129.
- Hinson, D. P., R. A. Simpson, J. D. Twicken, G. L. Tyler, and F. M. Flasar (1999), Initial results from radio occultation measurements with Mars Global Surveyor, *J. Geophys. Res.*, *104*, 26,997–27,012, doi:10.1029/1999JE001069.
- Holton, J. R. (2004), *An Introduction to Dynamic Meteorology*, 4th ed., 535 pp., Elsevier, Amsterdam.
- Holton, J. R., P. H. Haynes, M. E. McIntyre, A. R. Douglass, R. B. Rood, and L. Pfister (1995), Stratosphere-troposphere exchange, *Rev. Geophys.*, *33*(4), 403–439, doi:10.1029/95RG02097.
- Houben, H. (1999), Assimilation of Mars Global Surveyor meteorological data, *Adv. Space Res.*, *23*(11), 1899–1902, doi:10.1016/S0273-1177(99)00273-2.
- Jakosky, B. M., and T. Z. Martin (1987), Mars: North-polar atmospheric warming during dust storms, *Icarus*, *72*, 528–534, doi:10.1016/0019-1035(87)90050-9.
- Joshi, M. M., S. R. Lewis, P. L. Read, and D. C. Catling (1995), Western boundary currents in the Martian atmosphere: Numerical simulations and observational evidence, *J. Geophys. Res.*, *100*, 5485–5500, doi:10.1029/94JE02716.
- Kahre, M. A., J. R. Murphy, and R. M. Haberle (2006), Modeling the Martian dust cycle and surface dust reservoirs with the NASA Ames general circulation model, *J. Geophys. Res.*, *111*, E06008, doi:10.1029/2005JE002588.
- Kleinböhl, A., et al. (2009a), Mars Climate Sounder limb profile retrieval of atmospheric temperature, pressure, dust, and water ice opacity, *J. Geophys. Res.*, *114*, E10006, doi:10.1029/2009JE003358.
- Kleinböhl, A., et al. (2009b), Mars Climate Sounder limb retrievals of dust and water ice using scattering radiative transfer: Implications for particle size, paper presented at Mars Dust Cycle Workshop, NASA Ames Res. Cent., Mountain View, Calif., 15–17 Sept.
- Kuroda, T., N. Hashimoto, D. Sakai, and M. Takahashi (2005), Simulation of the Martian atmosphere using a CCSR/NIES AGCM, *J. Meteorol. Soc. Jpn.*, *83*(1), 1–19, doi:10.2151/jmsj.83.1.
- Kuroda, T., A. S. Medvedev, P. Hartogh, and M. Takahashi (2009), On forcing the winter polar warmings in the Martian middle atmosphere during dust storms, *J. Meteorol. Soc. Jpn.*, *87*(5), 913–921, doi:10.2151/jmsj.87.913.
- Lee, C., et al. (2009), Thermal tides in the Martian middle atmosphere as seen by the Mars Climate Sounder, *J. Geophys. Res.*, *114*, E03005, doi:10.1029/2008JE003285.
- Leovy, C. B. (1964), Simple models of thermally driven mesospheric circulation, *J. Atmos. Sci.*, *21*, 327–341, doi:10.1175/1520-0469(1964)021<0327:SMOTDM>2.0.CO;2.
- Lewis, S. R., P. L. Read, B. J. Conrath, J. C. Pearl, and M. D. Smith (2007), Assimilation of thermal emission spectrometer atmospheric data during the Mars Global Surveyor aerobraking period, *Icarus*, *192*, 327–347, doi:10.1016/j.icarus.2007.08.009.
- Lindzen, R. S., and A. Y. Hou (1988), Hadley circulations for zonally averaged heating centered off the equator, *J. Atmos. Sci.*, *45*, 2416–2427, doi:10.1175/1520-0469(1988)045<2416:HCFZAH>2.0.CO;2.
- McCleese, D. J., J. T. Schofield, F. W. Taylor, S. B. Calcutt, M. C. Foote, D. M. Kass, C. B. Leovy, D. A. Paige, P. L. Read, and R. W. Zurek (2007), Mars Climate Sounder: An investigation of thermal and water vapor structure, dust and condensate distributions in the atmosphere, and energy balance of the polar regions, *J. Geophys. Res.*, *112*, E05S06, doi:10.1029/2006JE002790.
- McCleese, D. J., et al. (2008), Intense polar temperature inversion in the middle atmosphere on Mars, *Nat. Geosci.*, *1*, 745–749, doi:10.1038/ngeo332.
- McCleese, D. J., et al. (2010), Structure and dynamics of the Martian lower and middle atmosphere as observed by the Mars Climate Sounder: Seasonal variations in zonal mean temperature, dust and water ice aerosols, *J. Geophys. Res.*, *115*, E12016, doi:10.1029/2010JE003677.
- Miyahara, S., Y. Yoshida, and Y. Miyoshi (1993), Dynamic coupling between the lower and upper atmosphere by tides and gravity waves, *J. Atmos. Terr. Phys.*, *55*, 1039–1053, doi:10.1016/0021-9169(93)90096-H.
- Moudden, Y., and J. C. McConnell (2005), A new model for multiscale modeling of the Martian atmosphere, GM3, *J. Geophys. Res.*, *110*, E04001, doi:10.1029/2004JE002354.
- Murphy, J. R., R. M. Haberle, O. B. Toon, and J. B. Pollack (1993), Martian global dust storms: Zonally symmetric numerical simulations including size-dependent particle transport, *J. Geophys. Res.*, *98*, 3197–3220, doi:10.1029/92JE02945.
- Richardson, M. I., and R. J. Wilson (2002), A topographically forced asymmetry in the Martian circulation and climate, *Nature*, *416*(6878), 298–301, doi:10.1038/416298a.
- Richardson, M. I., R. J. Wilson, and A. V. Rodin (2002), Water ice clouds in the Martian atmosphere: General circulation model experiments with a simple cloud scheme, *J. Geophys. Res.*, *107*(E9), 5064, doi:10.1029/2001JE001804.
- Richardson, M. I., A. D. Toigo, and C. E. Newman (2007), PlanetWRF: A general purpose, local to global numerical model for planetary atmospheric and climate dynamics, *J. Geophys. Res.*, *112*, E09001, doi:10.1029/2006JE002825.
- Schneider, E. K. (1983), Martian great dust storms: Interpretive axially symmetric models, *Icarus*, *55*, 302–331, doi:10.1016/0019-1035(83)90084-2.
- Smith, M. D., J. C. Pearl, B. J. Conrath, and P. R. Christensen (2001), Thermal Emission Spectrometer results: Mars atmospheric thermal structure and aerosol distribution, *J. Geophys. Res.*, *106*, 23,929–23,945, doi:10.1029/2000JE001321.
- Sprague, A. L., W. V. Boynton, K. E. Kerry, D. M. Janes, N. J. Kelly, M. K. Crombie, S. M. Nelli, J. R. Murphy, R. C. Reedy, and A. E. Metzger (2007), Mars' atmospheric argon: Tracer for understanding Martian atmospheric circulation and dynamics, *J. Geophys. Res.*, *112*, E03S02, doi:10.1029/2005JE002597.
- Takahashi, Y. O., H. Fujiwara, H. Fukunishi, M. Odaka, Y.-Y. Hayashi, and S. Watanabe (2003), Topographically induced north-south asymmetry of the meridional circulation in the Martian atmosphere, *J. Geophys. Res.*, *108*(E3), 5018, doi:10.1029/2001JE001638.

- Wallace, J. M., and P. V. Hobbs (1976), *Atmospheric Science: An Introductory Survey*, 467 pp., Academic, San Diego, Calif.
- Wilson, R. J. (1997), A general circulation model simulation of the Martian polar warming, *Geophys. Res. Lett.*, *24*(2), 123–126, doi:10.1029/96GL03814.
- Wilson, R. J., and K. Hamilton (1996), Comprehensive model simulation of thermal tides in the Martian atmosphere, *J. Atmos. Sci.*, *53*, 1290–1326, doi:10.1175/1520-0469(1996)053<1290:CMSOTT>2.0.CO;2.
- Wilson, R. J., D. Banfield, B. J. Conrath, and M. D. Smith (2002), Traveling waves in the northern hemisphere of Mars, *Geophys. Res. Lett.*, *29*(14), 1684, doi:10.1029/2002GL014866.
- Wilson, R. J., S. R. Lewis, L. Montabone, and M. D. Smith (2008), Influence of water ice clouds on Martian tropical atmospheric temperatures, *Geophys. Res. Lett.*, *35*, L07202, doi:10.1029/2007GL032405.
- Zalucha, A. M., R. A. Plumb, and R. J. Wilson (2010), An analysis of the effect of topography on the Martian Hadley cells, *J. Atmos. Sci.*, *67*, 673–693, doi:10.1175/2009JAS3130.1.
- Zurek, R. W. (1992), Comparative aspects of the climate of Mars: An introduction to the current atmosphere, in *Mars*, edited by H. H. Kieffer et al., pp. 799–817, Univ. of Ariz. Press, Tucson.
- Zurek, R. W., and S. E. Smrekar (2007), An overview of the Mars Reconnaissance Orbiter (MRO) science mission, *J. Geophys. Res.*, *112*, E05S01, doi:10.1029/2006JE002701.
- Zurek, R. W., J. R. Barnes, R. M. Haberle, J. B. Pollack, J. E. Tillman, and C. B. Leovy (1992), Dynamics of the atmosphere of Mars, in *Mars*, edited by H. H. Kieffer et al., pp. 835–933, Univ. of Ariz. Press, Tucson.
-
- N. G. Heavens, Department of Earth and Atmospheric Sciences, Cornell University, 1118 Bradfield Hall, Ithaca, NY 14853, USA. (heavens@cornell.edu)
- D. M. Kass, A. Kleinböhl, D. J. McCleese, and J. T. Schofield, Jet Propulsion Laboratory, California Institute of Technology, 4800 Oak Grove Dr., Pasadena, CA 91109, USA.
- M. I. Richardson, Ashima Research, 600 S. Lake Ave., Ste. 303, Pasadena, CA 91106, USA.